

# Self-Lifting Unmanned Aerial Aircraft

Design Patent for this project:-



# Table of Contents

Nomenclature.....	4
1. Abstract.....	5
2. Introduction.....	5
3. Aircraft Configuration.....	6
3.1. Wing .....	6
3.1.1. Airfoil Selection .....	6
3.1.2. Configuration.....	7
3.2. Fuselage .....	8
3.2.1. Airfoil Selection .....	8
3.2.2. Configuration.....	9
3.3. Empennage.....	9
3.3.1. Airfoil Selection .....	9
3.3.2. Configuration.....	11
3.3.3. Tail Positioning w.r.t fuselage.....	11
3.3.4. Elevator and Rudder Design .....	12
4. Wing Detailed Design .....	12
4.1. Wing loading:.....	12
4.2. Wing design parameters.....	12
4.2.1. Aspect ratio .....	12
4.2.2. Wing planform.....	13
4.2.3. Aileron and winglets.....	13

4.2.4. Wingtip fence .....	14
5. Design Analysis and Performance optimization.....	15
6. Stability Analysis .....	17
6.1. Aerodynamic center, Centre of Gravity and Neutral point.....	17
6.2. Static Margin.....	17
6.3. Longitudinal Stability .....	18
6.4. Lateral stability.....	20
6.5. Directional stability .....	22
7. Power Plant Performance .....	23
7.1. Motor & Propeller Selection .....	23
7.2. Battery Selection .....	24
7.3. ESC Selection.....	24
7.4. Servo Sizing .....	25
8. Payload prediction.....	26
8.1. Conclusion .....	26
9. Rib Spacing and Spar Location: .....	27
10. 2D Drawing.....	28
11. Conclusion .....	29
References .....	29

## Nomenclature

Symbol	Name	Symbol	Name
$MAC$	Mean aerodynamic chord	$RPM$	Motor Rotation per minute
$Cl$	Coefficient of Lift	$F$	Dynamic Thrust
$Cd$	Coefficient of Drag	$d$	Diameter of propeller
$Cm$	Coefficient of Pitching Moment	$V_0$	Aircraft speed
$\alpha$	Angle of Attack	$T_{flight}$	Time of flight
$\overline{C}_W$	MAC of the wing	$c$	Control surface chord length
$V_H$	Volume coefficient of horizontal tail	$L$	Length of control surface
$V_V$	Volume coefficient of vertical tail	$v$	Aircraft cruise speed
$d$	Downwash angle at cruise condition	$\emptyset$	Maximum deflection
$H$	Vertical distance below the tail MAC between wake displacement line and fuselage reference line	$\omega_n$	Natural frequency
$M$	Vertical distance between the fuselage reference line and the tail position	$\omega_1$	Damped natural frequency
$\frac{W}{S}$	Wing Loading	$\xi$	Damping constant
$S_{land}$	Landing Distance	$X$	Horizontal distance between the wing MAC and the tail MAC
$Cl_{max}$	The maximum coefficient of lift	$Cn$	Yawing moment coefficient
$\rho_0$	Air density at sea level	$T_m$	Air temperature at given altitude (K)
$\sigma$	The altitude of the landing field	$T_b$	Base temperature
$\beta$	sideslip angle	$L_b$	The base temperature lapse rate
		$P_b$	Base static pressure
		$P_a$	The actual pressure in inches Hg

## **1. Abstract**

The SAE ISS Aero design competition is an excellent forum for aspiring engineers to gain a deep understanding of the design and fabrication facets of aero-modelling, which enables students to improve team-building skills. This competition provides team members with realistic hands-on training with both designing and operating aircrafts. The motive of this competition, is to manufacture a remote-controlled aircraft which is able to lift as much weight while staying within the competition's constraints. The accompanying article summarizes the project's review, substantiation, and final performance.

## **2. Introduction**

Team Phoenix Aero was established in 2019 by a group of committed aero enthusiasts from Sardar Vallabhbhai National Institute of Technology (SVNIT), Surat who shared a dream of designing and competing in the coveted SAE ISS Aero design challenge.

This design report has been produced by Phoenix Aero in order to compete in the SAE ISS Aero design 2021 competition in the regular class division. The key goal is to design and develop an unmanned aerial vehicle capable of carrying the maximum cargo possible. The team has developed a unique self-lifting fuselage design that is more aerodynamic in nature. To produce the maximum lift, a high camber airfoil coupled with a semi taper rectangular planform is used. For the empennage, it was chosen to use a U-Tail configuration for enhanced stability. It must also complete its mission while adhering to SAE design specifications and being a stable aircraft to fly.

### 3. Aircraft Configuration

#### 3.1. Wing

##### 3.1.1. Airfoil Selection

The selection of airfoil for the wing was made keeping in mind the objective of the competition. The aircraft is flying at low altitudes and low speed, so the analysis was done for Reynolds Number below 500,000. The airfoil chosen has to have a high camber to provide a higher lift. Two Airfoils, i.e., E423 and S1210, met the requirement needed for the aircraft. On analysis, S1210 and E432 showed similar results. At the lower angle of attacks, S1210 has lower  $C_l$  than its E423.

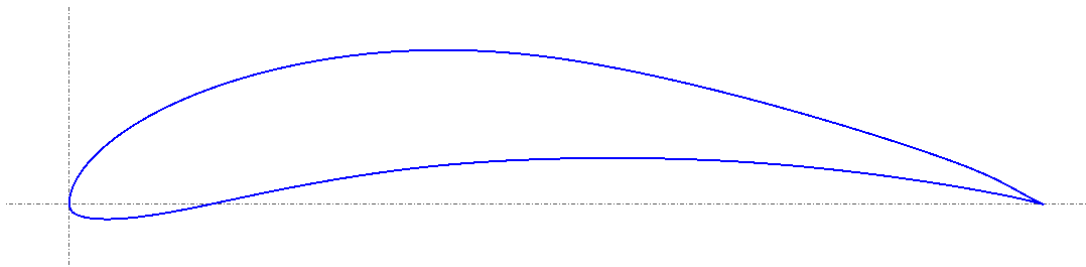


**Figure I** E423

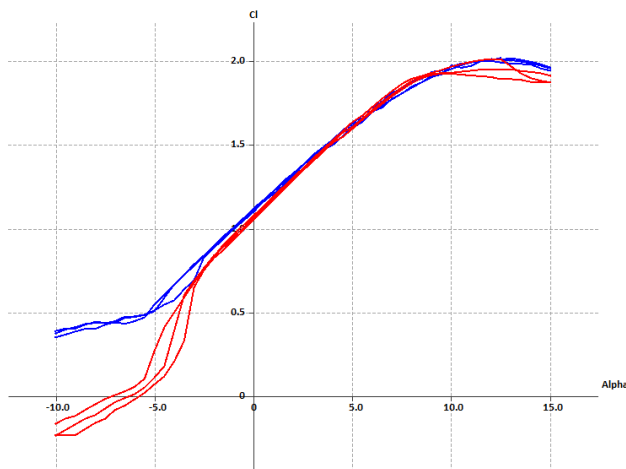


**Figure II**  $C_l$  v/s  $\alpha$

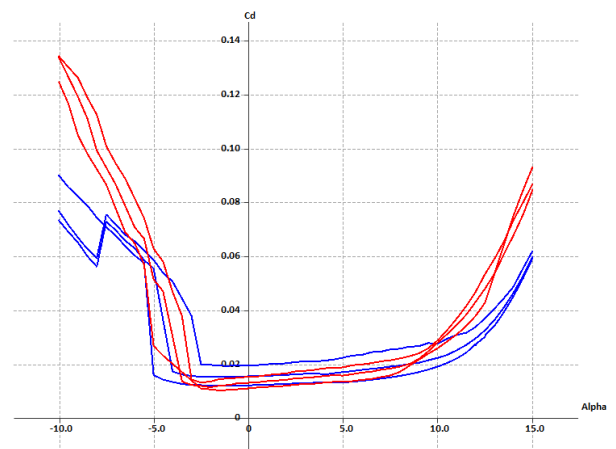


**Figure III**  $C_d$  v/s  $\alpha$

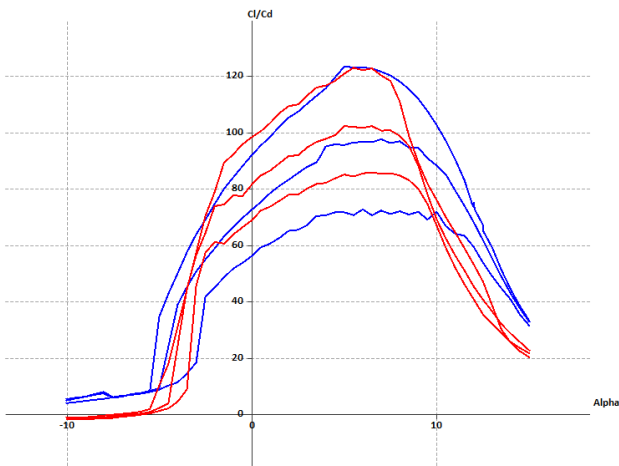


**Figure IV** Cl/Cd v/s  $\alpha$

S1210 —————

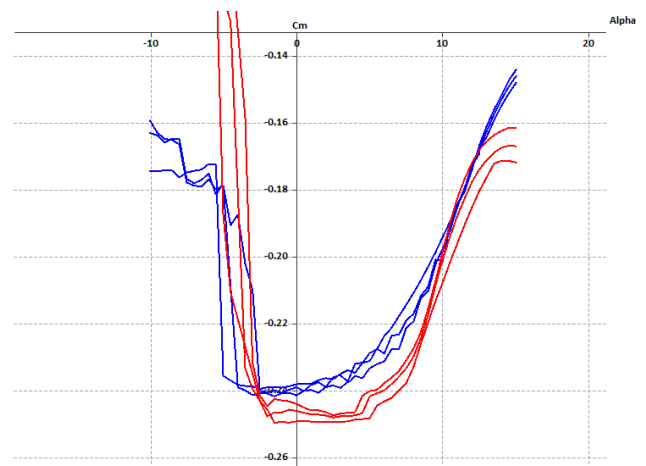


**Figure V** Cm v/s  $\alpha$

E423 —————

Similarly, In Figure III , S1210 has a higher drag coefficient at the negative angle of attack. Even though S1210 excelled in some areas, it has a really thin trailing edge which would cause a problem for the aluminum rods, which is to be connected to the fuselage. E423 was found to be the right choice for the aircraft.

### 3.1.2. Configuration

The concept of the self-lifting fuselage is used in this aircraft. Due to this, the shape of the fuselage is an Airfoil shape. This cuts down the possibilities of having a high or a low wing configuration as it would not provide enough mounting strength to the wing onto the fuselage. Shoulder wing configuration was selected as it shares some characteristics of high wing and mid-wing configurations <sup>[1]</sup> It requires no wing dihedral for providing lateral stability like the high wing, and aerodynamically it is streamlined like the mid-wing configuration. Keeping all these factors into consideration, shoulder-wing configuration was selected.

### 3.2. Fuselage

#### 3.2.1. Airfoil Selection

The selection of airfoil for the fuselage is made keeping in mind the size of the payload bay. The airfoil chosen should be thick and have a high camber that can easily fit a payload bay of height and width of 4 inches. It was determined that the airfoil has to have a thickness greater than 18% and camber around 40%. The two airfoils shortlisted on this basis were Eppler 604 and GOE 382.

**Table I.** Shortlisted Airfoils for Fuselage

Airfoil	Maximum Thickness	Maximum Camber
Eppler 604	19.8% at 37.3% of the chord	3.4% at 42.3% of chord
GOE 382	20% at 29% chord	6% at 39% of chord

Batch Analysis was done using xflr5 for the above two shortlisted Airfoils.

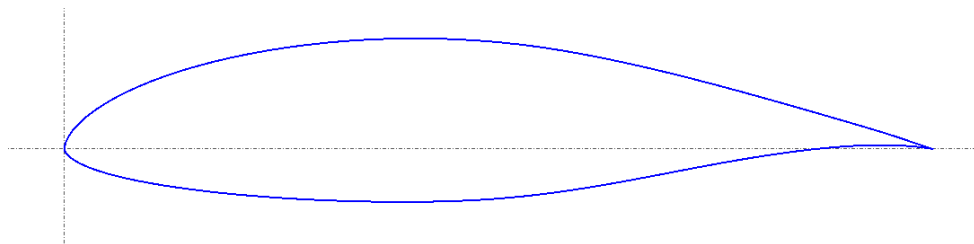


**Figure VI** Eppler 604

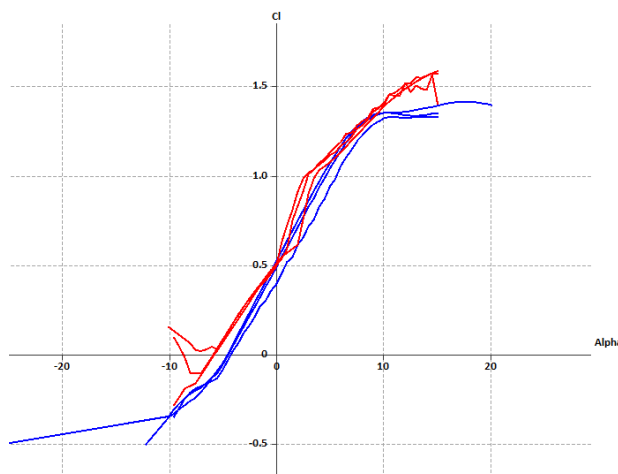


**Figure VII** Cl v/s  $\alpha$

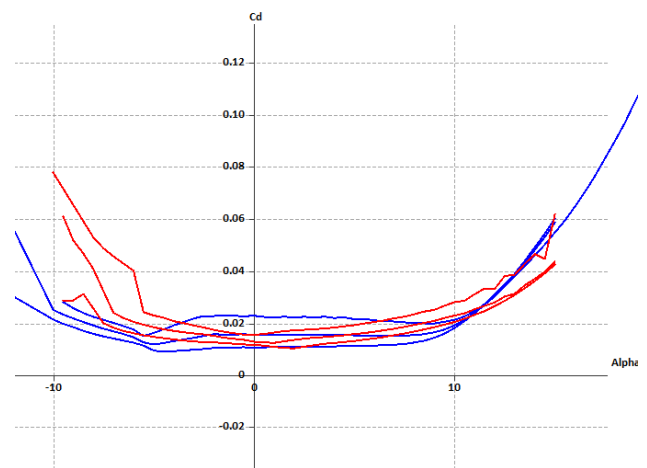


**Figure VIII** Cd v/s  $\alpha$

GOE 382 —————

Eppler 604 —————

It is observed that Eppler 604 has a larger stall angle compared to GOE 382.  $C_l$  of Eppler 604 is lesser than GOE 382, but it has a smoother curve that would provide a stable lift to the aircraft than the other airfoil. The drag bucket of the Eppler 604 is also seen wider than GOE 382, which gives it an upper hand in drag minimization. Eppler 604 proved to be the right choice for the fuselage.

### 3.2.2. Configuration

The fuselage configuration is an essential aspect of the aircraft's architecture. The team wanted to increase lift while lowering drag and making the aircraft more aerodynamic. The fuselage's shape was designed as an airfoil to reduce drag and make the fuselage more aerodynamic. Since the wing configuration is a shoulder wing, a gradient was maintained on the fuselage's sides to maintain its aerodynamic shape.

### 3.3. Empennage

#### 3.3.1. Airfoil Selection

Among various airfoils, Joukowski-12 and Naca0012 were shortlisted. The most suitable airfoil for the empennage was Joukowski-12 because it has a slightly higher  $C_l$  v/s  $C_d$  coefficient curve and a docile peak of the lift-curve slope, emphasizing that beyond the stall angle, the  $C_l$  will not decrease suddenly. This is beneficial for the safe flight of the aircraft. Also, the stall angle was maximum for Joukowski-12 among all airfoils of similar thickness, and the peak of  $C_l$  v/s  $\alpha$  is docile, hence avoiding the sudden stall of the tail.

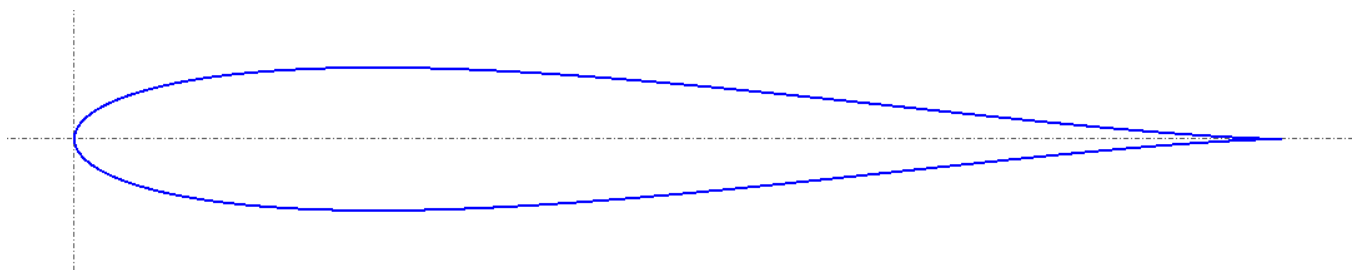


**Figure IX** Joukowski-12

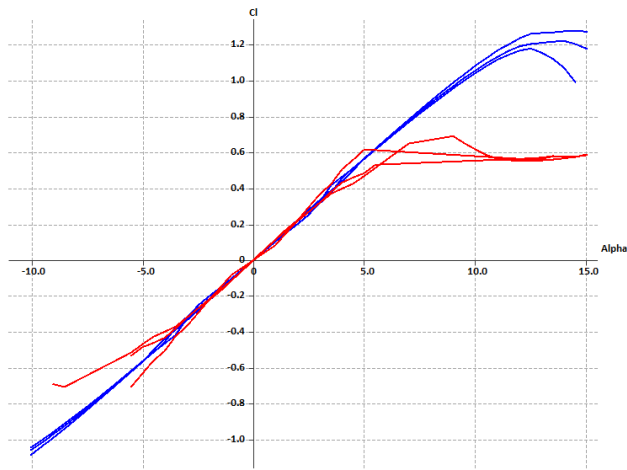


**Figure X**  $C_l$  v/s  $\alpha$

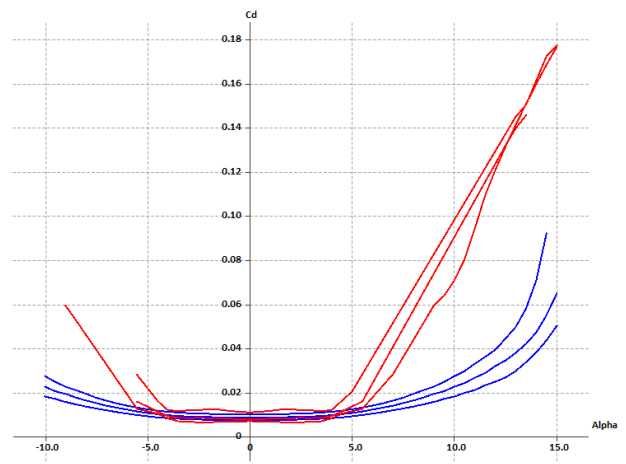


**Figure XI**  $C_d$  v/s  $\alpha$

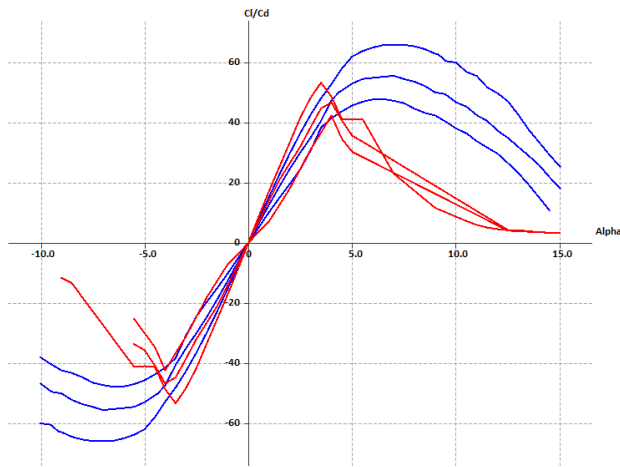


**Figure XII**  $C_l/C_d$  v/s  $\alpha$

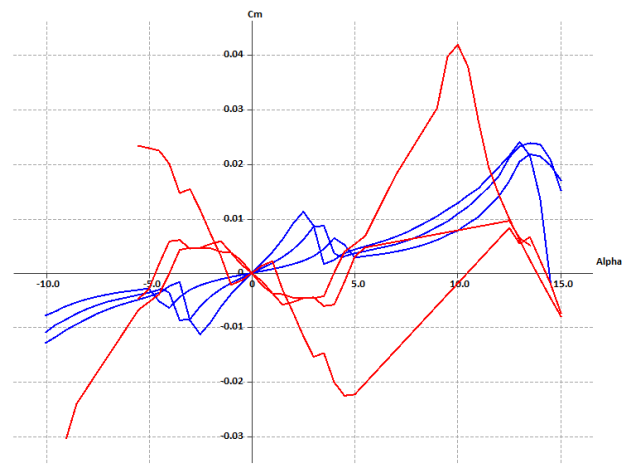


**Figure XIII**  $C_m$  v/s  $\alpha$

NACA 0012 —————

Joukowski-12 —————

From the  $C_l$  v/s  $\alpha$  graph, the lift increased/decreased smoothly with change  $\alpha$ , thus giving better predictability of lift. Simultaneously, the graph of  $C_l/C_d$  v/s  $\alpha$  of the airfoil shows a good aerodynamic efficiency given by the ratio of  $C_l/C_d$  v/s  $\alpha$  at a constant velocity and density. The pitching moment has minimum fluctuation and lower peaks of  $C_m$ , providing better maneuverability. Additionally, the curve deviated very little in  $C_m$ 's negative values for a positive  $\alpha$  at low Reynolds Number, and for a higher Reynolds Number, the curve tends to be positive.

### 3.3.2. Configuration

Among various empennage configurations available, U-tail was chosen as the final configuration because the positioning of the two vertical stabilizers at the ends of the horizontal stabilizer allows for a smaller, lighter, and more aerodynamically efficient horizontal stabilizer with smooth weight distribution<sup>[2]</sup> Considering the aircraft's pitch behavior, stability and controllability,  $V_V$  was concluded as 0.04 and  $V_H$  to be 0.57<sup>[3]</sup> The horizontal tail's aspect ratio was determined by considering its bending moment and finalized as 3.61<sup>[3]</sup> The tip effect and control of the vertical tail increase by increasing the aspect ratio, so the aspect ratio of the vertical tail was finalized as 1.6

### 3.3.3. Tail Positioning w.r.t fuselage

The tail is affected by the wing's wake and downwash, which results in a decrease in  $\alpha$ . This can be resolved by tail positioning, which is done by keeping the tail at a vertical distance of half the wing MAC from the wake displacement line, i.e.,  $M + H = \frac{\bar{C}_w}{2}$  as shown in Figure XIV .

Downwash data was calculated from wing parameters for different angles of attack of the wing to obtain vertical height as follows:

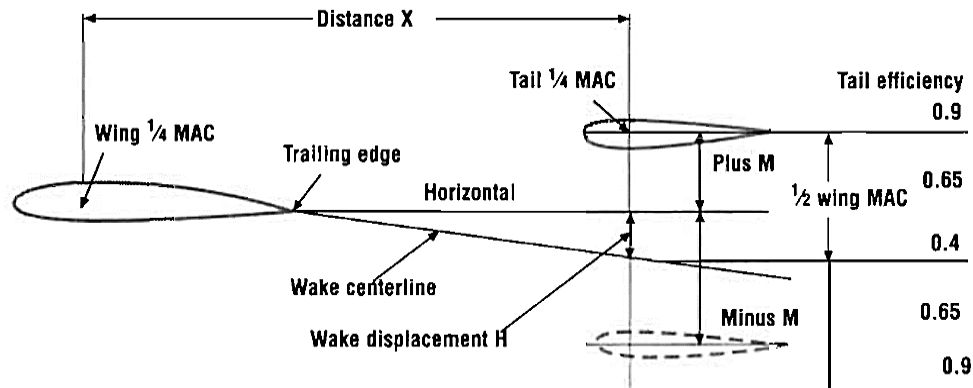


Figure XIV Wake and Downwash Determination<sup>[4]</sup>

Table II. Vertical Height Calculation

Wake displacement H	$(X - 0.7 * CW) * \tan d$	0.0352 m
Vertical Height of Tail M	$\frac{\bar{C}_W}{2} - H$	0.0883m

### 3.3.4. Elevator and Rudder Design

For appropriate controllability and stability, the elevator area was finalized as 33% of the horizontal stabilizer area. A rectangular configuration-type rudder was chosen. For appropriate controllability and stability, the rudder area was chosen as 40% of the vertical stabilizer area. A taper cut was made on the rudder for undisturbed movement of the elevator.

## 4. Wing Detailed Design

### 4.1. Wing loading:

Wing loading is the total weight of an aircraft divided by the area of its wing. Estimation of wing loading for an aircraft is crucial since it influences several performance parameters such as stalling speed, take-off and landing distance, maneuverability, stability, etc. Its value was estimated using the following relationship between wing loading and landing distance of aircraft <sup>[1]</sup>

$$\frac{W}{S} = 0.8563 * C_l^{max} * S_{land} * \rho_0 * \sigma$$

The selected wing loading for the given aircraft is  $155 \text{ N/m}^2$  for a landing distance of 250 ft.

### 4.2. Wing design parameters

#### 4.2.1. Aspect ratio

The aspect ratio is the primary factor in determining the ordinary wing's three-dimensional characteristics and its lift/drag ratio <sup>[4]</sup> Since the aircraft is proposed to have a high lifting capacity, the aspect ratio (AR) needs to be high. This will increase the endurance slightly and give us a high Cl/Cd ratio. High aspect ratio wings have longer wingspan. So, the AR is chosen near to 9 and 9.5.

**Table III.** Aspect Ratio Calculations

Mass (kg)	Wing Area (m <sup>2</sup> )	Aspect ratio	
		9	
		Wingspan (m)	Avg. Chord length (m)
10	0.613166216	2.349147918	0.261016435
11	0.674482837	2.463807123	0.273756347
12	0.735799459	2.573362612	0.285929179

#### 4.2.2. Wing planform

The tapered wing planform has the wing narrow towards the tip. Structurally and aerodynamically, it is more efficient than a constant chord wing and more manageable to construct than the elliptical type. The tapering causes a decrease in drag (most effective at high speeds) and increased lift. The planform design is concluded to be a tapered type.

The graphs are analyzed for different values of X and compared with the elliptical planform characteristics. The most efficient taper is selected as Sweep back of 12.03° with a taper ratio of 0.498.

#### 4.2.3. Aileron and winglets

The above calculations and after analysis in XFLR5 for Cl/Cd ratio, the aileron's dimensions are selected to have  $\delta = 0.9239$  for  $C = 0.228$  <sup>[5]</sup> According to dimensions and the XFLR simulation, the aileron's position is shown in Figure XV for the decided planform design.



## 5. Design Analysis and Performance optimization

A three-dimensional CFD analysis was done on ANSYS FLUENT to check how the aircraft would perform in the real world. The analysis was performed to compute the lift and drag forces along with their coefficients using a Solid works model of the aircraft, which was imported into ANSYS workbench and was then finely meshed using the Sphere of Influence sizing method with local origin at the center of the aircraft. The K-Epsilon turbulence model was used to compute the simulation, which uses two transport equations with the variable being turbulent kinetic energy (K) and rate of dissipation of turbulent kinetic energy (Epsilon), and the following initial conditions were specified:

**Table IV.** Specified initial conditions

<b>Parameter</b>	<b>Specified condition</b>	
<b>Fluid</b>	Air	Density= 1.225 Kg/m <sup>3</sup> Viscosity= 1.7894×10 <sup>-5</sup> N.s/m <sup>2</sup>
<b>Solid aircraft body</b>	Balsa wood	Density= 250 Kg/m <sup>3</sup>
<b>Inlet</b>	Velocity Inlet	Magnitude= 15.41 m/s
<b>Outlet</b>	Pressure Outlet	Gauge pressure= 0 Pascal
<b>Temperature</b>	Ambient	293.15 Kelvin
<b>Angle of attack</b>	15 degrees (Approximate stall angle)	

The following simulation results were computed for 1000 iterations specified to the solver along with report definitions specified to calculate lift and drag:

**Table V.** Lift and drag forces.

Serial No.	Force	Value	Direction (w.r.t. Global coordinates)
1.	Drag	30.4277 Newton	Along the positive X-axis
2.	Lift	149.80435 Newton	Along the positive Y-axis

**Table VI.** Coefficients of forces

Serial No.	Coefficient	Computed value
1.	Coefficient of drag (Cd)	49.677915
2.	Coefficient of lift (Cl)	244.57853

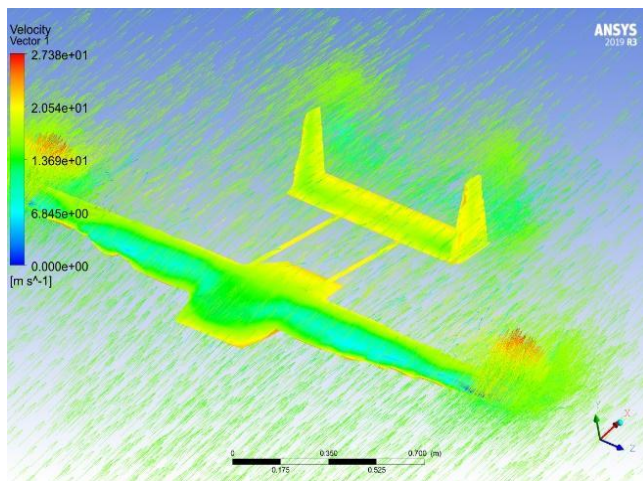


**Figure XVII** Velocity vector distribution around aircraft

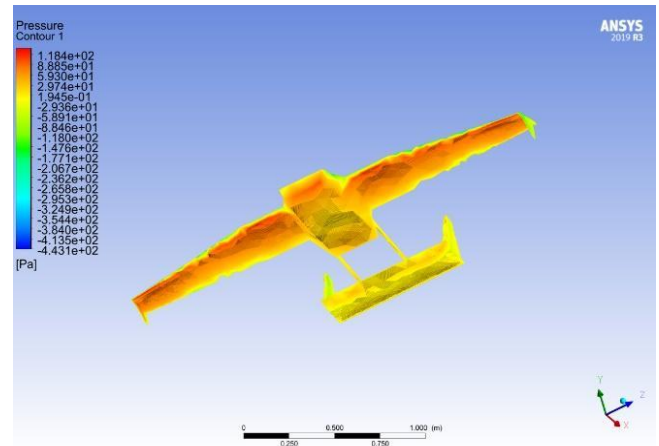


**Figure XVIII** Pressure contour distribution around the aircraft

The simulation was computed for various angles of attacks and the maximum lift was obtained for around 15 degrees which is supposed to be the stall angle. The computed lift value is more than enough to carry the predicted payload value with the least drag.

## 6. Stability Analysis

### 6.1. Aerodynamic center, Centre of Gravity and Neutral point

**Table VII.** Positioning of various important points

Name	Coordinates (in mm)	Distance from the nose of the aircraft (in mm)
Aerodynamic center (AC)	(356.21, 0, 0)	356.21
Neutral point (NP)	(301, 0, 0)	301
Centre of gravity (CG) (without payload)	(297.63, 12.36, 12.24)	298.13
Centre of gravity (CG) (with a payload of 7.8* Kgs)	(274.46, 6.87, 3.51)	274.51

\*Payload of 7.8 Kgs is added here, making the maximum assumed aircraft weight to be 11 Kgs.

**Table VIII.** The range of variation of center of gravity

Direction	Location variation	Range (in mm)
Along X (in mm)	297.63 – 274.46	23.17
Along Y (in mm)	12.36 – 6.87	5.49
Along Z (in mm)	12.24 – 3.51	8.74

### 6.2. Static Margin

Mean Aerodynamic Chord (MAC) = 0.375m

Static Margin without payload =  $\left[ \frac{(NP-CG)}{MAC} \right] \times 100\%$

$$= \left[ \frac{(0.301 - 0.29763)}{0.375} \right] \times 100\%$$

$$= 0.8986 \% \text{ of } MAC$$

$$\begin{aligned} \text{Static margin with a payload of 7.8 kg} &= \left[ \frac{(NP-CG)}{MAC} \right] \times 100\% \\ &= \left[ \frac{(0.301 - 0.27446)}{0.375} \right] \times 100\% \\ &= 7.07733\% \text{ of } MAC \end{aligned}$$

### 6.3. Longitudinal Stability

Longitudinal stability is the tendency of an aircraft to return to the trimmed angle of attack. Also, the longitudinal stability of the aircraft improves with the static stability margin. As the Static margin is 7.6% within the recommended range of 5% to 10% [7] longitudinal stability is satisfied with this criterion.

**Table IX.** Values calculated for longitudinal static stability

Criteria	Analysis value
$C_{m\alpha} = \frac{dC_m}{d\alpha} < 0$	-0.00703
$C_{m_0} > 0$	-0.05337

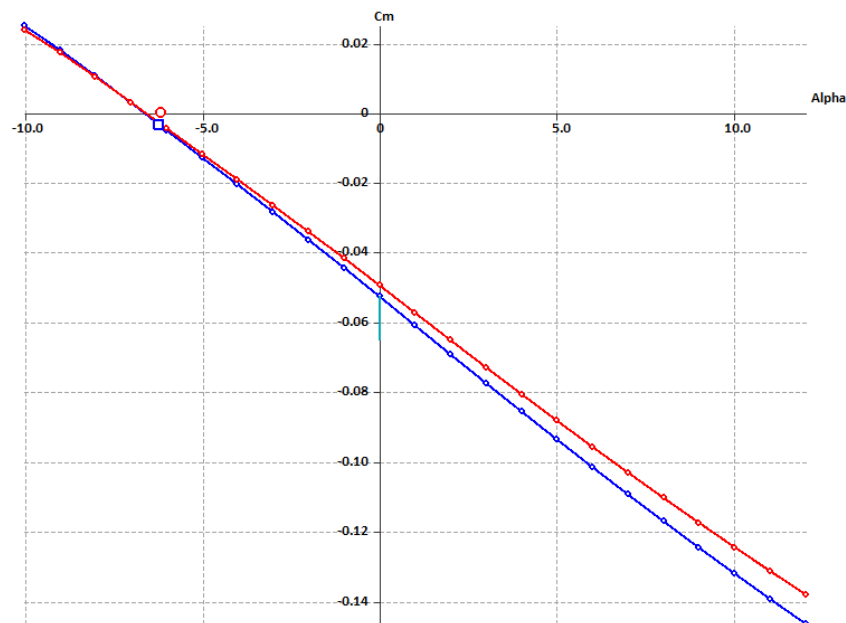


**Figure XIX** Cm v/s  $\alpha$  for the entire aircraft

Hence the plane is longitudinally stable.

**Table X.** Mode frequency for Longitudinal stability.

Mode	Response	Value
<b>Phugoid</b>	$\omega_n$	3.789 Hz
	$\omega_1$	1.981 Hz
	$\tau$	0.852
<b>Short Periods</b>	$\omega_n$	0.068 Hz
	$\omega_1$	0.041 Hz
	$\tau$	0.805

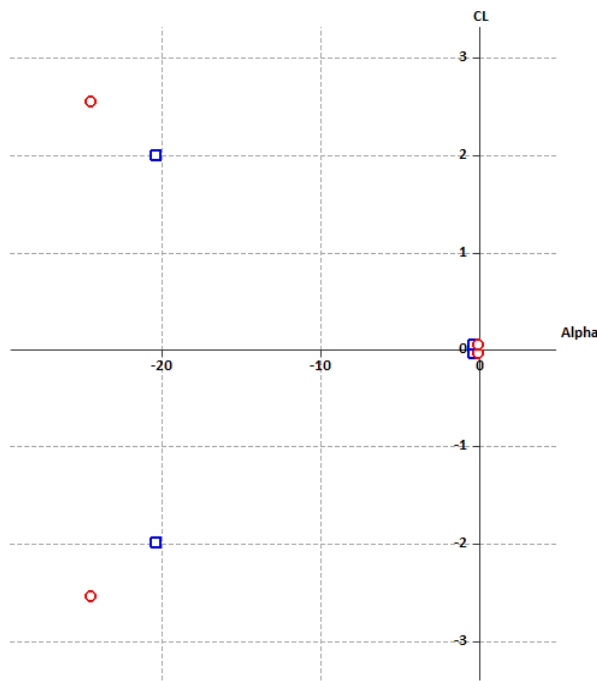


**Figure XX** Root Locus Graph

In the root locus graph for longitudinal modes, the left yellow nodes represent Phugoid mode response<sup>[7]</sup>  $\lambda$  and the right yellow nodes represent Short period mode response. Hence both modes are stable, with the phugoid response time being more (damping time more). Hence the aircraft is longitudinally dynamically stable.

## 6.4. Lateral stability

Lateral stability is the tendency of an aircraft to resist roll.

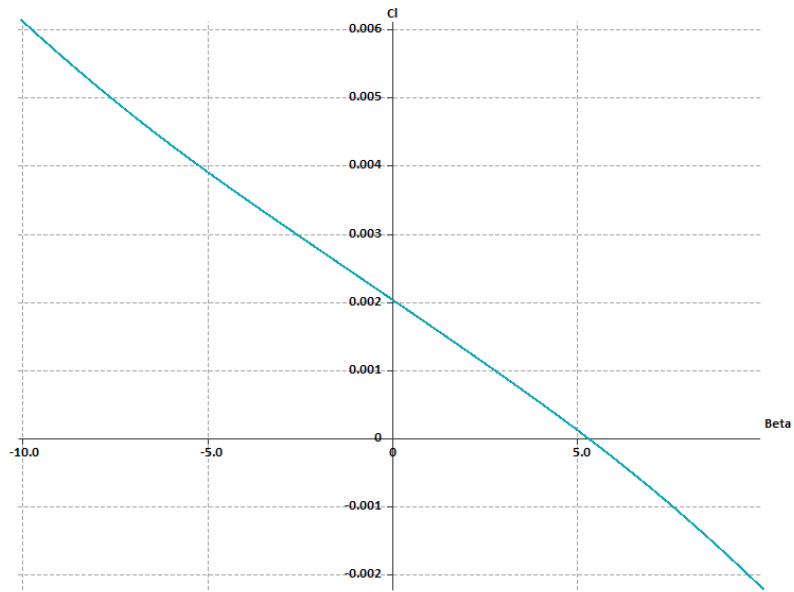


**Figure XXI** Cl v/s  $\beta$

**Table XI.** Values calculated for lateral stability

Criteria	Analysis value
$C_{l\beta} < 0$ (vertical tail lift curve slope)	-0.00042

**Table XII.** Mode frequency for Lateral stability.

Mode	Response	Value
Roll Damping	$\xi$	0.015
	$t_2$	0.011s
Dutch roll	$\omega_n$	1.765 Hz
	$\omega_1$	1.744 Hz
	$\tau$	0.152
Spiral Roll	$t_2$	8.943 s

The plane is Laterally statically stable.

Lateral dynamic stability has three modes/motions for analysis. They are Spiral mode (non-oscillatory long-duration motion with Bank angle increasing and altitude of flight decreasing), Roll mode (short duration rolling motion), and Dutch roll mode (long duration oscillatory combined yawing-rolling motion). Lateral dynamic modes like Spiral mode and Dutch roll mode show dependence on the roll as well as yaw.

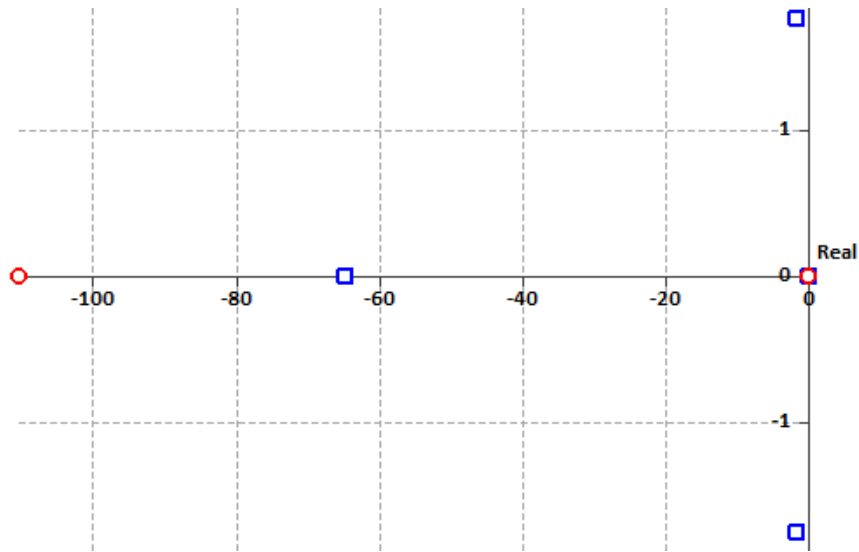


**Figure XXII** Root Locus Graph

As the value of damping constant  $\sigma$  becomes increasingly negative, the aircraft becomes more dynamically stable. Roll damping constant  $\sigma$  as leftmost locus point represents very high roll mode stability. Locus points with a magnitude around 1.65 show two symmetric Dutch roll mode response time and hence shows the Dutch roll stability. The spiral mode damping constant is very low but positive, indicating the aircraft's unstable spiral mode, common for many aircraft. The effect takes place over a long time and is negligible, and can often be corrected by the pilot easily. It can be concluded that aircraft is laterally dynamically stable.

## 6.5. Directional stability

Directional stability is the tendency of an aircraft to resist yaw.

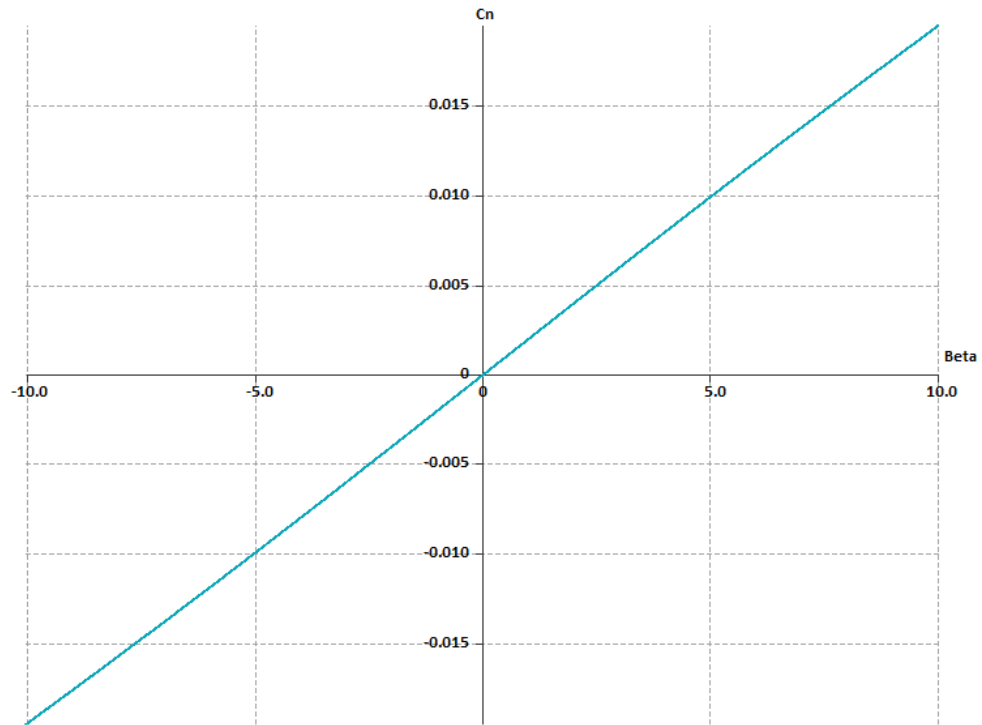


**Figure XXIII** Cn v/s  $\beta$

**Table XIII.** Values calculated for directional static stability

Criteria	Analysis value
$C_n\beta = \frac{dC_n}{d\beta} > 0$	0.001947

From the above results, the plane is directionally and statically stable.

## 7. Power Plant Performance

### 7.1. Motor & Propeller Selection

The BLDC motor and propeller are selected based on the thrust requirements and stalling speed of the aircraft. Required thrust was estimated by assuming a proper thrust/weight ratio.

$$\frac{\text{Thrust}}{\text{Weight}} (\text{with payload}) = 0.3$$

$$\frac{\text{Thrust}}{\text{Weight}} (\text{without payload}) = 0.75$$

The estimated aircraft weight with payload is 12kg.

$$\text{Estimated Thrust} = 12 \times 0.3 \times 1000 \text{ g} = 3600 \text{ g}.$$

BLDC motors fulfilling the thrust requirement with their suitable propeller were shortlisted. For propeller selection, stalling speed of the aircraft was considered, which is 11.42 m/s. The pitch speed of propeller can be given by,

$$\text{pitch speed} \geq 2.5 \times \text{stalling speed}$$

$$\text{pitch speed} \geq 28.55 \text{ m/s}$$

Pitch speed of propeller rotating with a given RPM can be provided by,

$$\text{pitch speed} = \frac{\text{RPM}}{60} \times \text{pitch (in)} \times \frac{2.54}{100} \text{ m/s}$$

**Table XIV.** Specifications of the selected motor and propeller

<b>Motor KV</b>	<b>Amp</b>	<b>Battery voltage (V)</b>	<b>Motor RPM</b>	<b>Propeller Diameter (in)</b>	<b>Propeller pitch (in)</b>	<b>Static thrust (N)</b>	<b>Pitch speed (m/s)</b>
540	46.55	18.5	8200	14	8.5	37.4256	29.50633

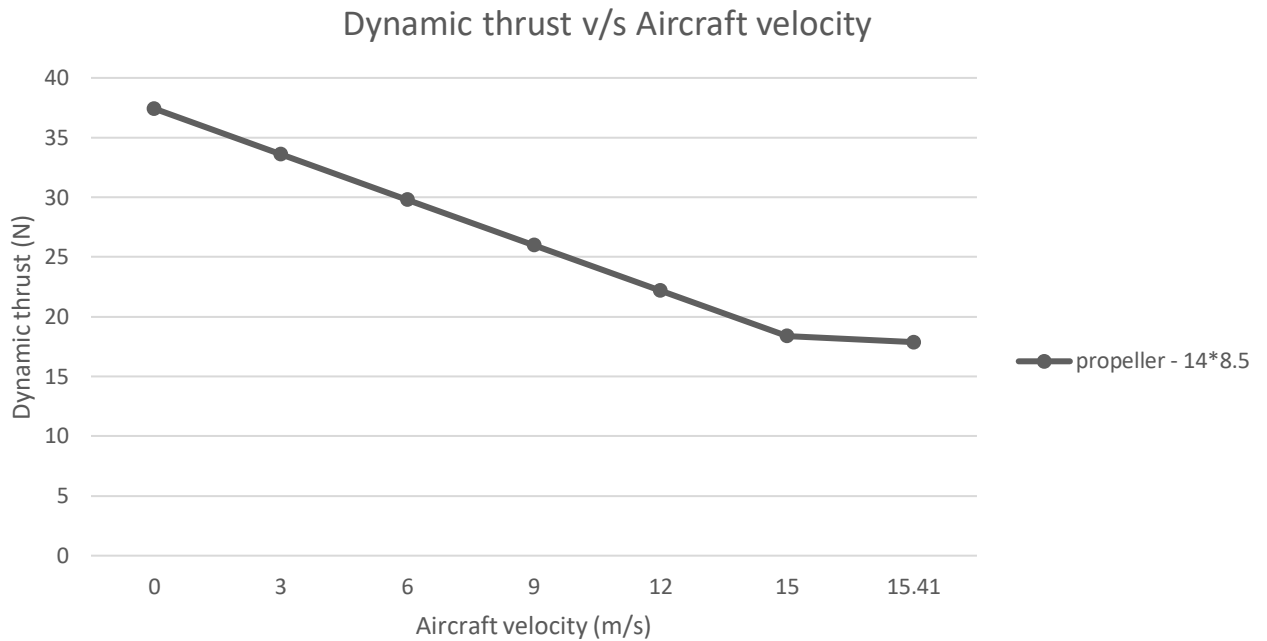


**Figure XXIV** The dynamic thrust for the selected motor and propeller at different aircraft speeds ( $V_0$ )

$$F = 4.392399 \times 10^{-8} \times RPM \times \frac{d^{3.5}}{\sqrt{pitch}} \times (4.23333 \times 10^{-4} \times RPM \times pitch - V_0) \text{ [8]}$$

## 7.2. Battery Selection

According to the rulebook, the lithium polymer battery pack of 4cell (14.8V) to 6cell (22.2V) Voltage rating can only be selected. Batteries were shortlisted according to the Voltage required by the selected motor (540 KV), and the one giving the highest Time of flight was selected.

$$Endurance = \frac{Capacity \times Discharge}{Average Amp Drawn}$$

The selected battery pack weighs 621g and has an endurance of 3 minutes 9.4737 seconds.

## 7.3. ESC Selection

The ESC selection was based on the ampere requirement of the BLDC motor. The ESCs were shortlisted to have a peak current of more than 20-25% of the motors' current requirement. The selected ESC has a burst ampere 80A and maximum RPM for two-pole motors of 240000.

#### 7.4. Servo Sizing

A total of 5 servos are selected (2 for ailerons, 2 for rudders, and 1 for elevator). Servos were selected based on the torque created by the drag force's opposing moment on the control surfaces. The torque required to maintain a control surface at equilibrium position is calculated by

The Chuck Gadd's torque equation:

$$\text{Torque (oz - in)} = 8.5 \times 10^{-6} \times (cv)^2 L \sin \phi^{[10]}$$

Considering Cruise speed of aircraft ( $v$ ) = 34.47427 mph.

**Table XV.** Servo requirements of control surfaces

<b>Control Surface</b>	<b>Maximum deflection (<math>\phi</math>) in degrees</b>	<b>Chord length (c) in cm</b>	<b>Length (L) in cm</b>	<b>Torque in oz - in</b>	<b>Torque in kg-cm</b>
Aileron	22	4.56	30.89	4.507419962	0.3245693
Elevator	22	7.23	79.14	29.03040339	2.09041516
Rudder	22	7.23	28.91	10.60486432	0.76363283

Based on the torque values and keeping a safety factor of 2-2.5, the servo motors for ailerons, elevators, and the rudder were selected.

## 8. Payload prediction

Payload prediction includes deriving a relation between payload (lbs.) and density altitude (ft). It indicates how much payload the aircraft would be able to carry at different densities of air. It was calculated assuming lift varied linearly with the density for cruise condition. The density, in turn, was varied according to altitude, with density altitude as a parameter. Following are the set of equations used to calculate payload prediction by using the relations between atmospheric parameters [9]

$$T_m = T_b + L_b(H - H_b)$$

$$\text{Density altitude} = 145442.16 * (1 - (17.326 * \frac{Pa}{T_r})^{0.235})$$

$$P = P_b \left( \frac{T_m}{T_b} \right)^{\frac{gM}{RL_b}}$$

$$\rho = \frac{P}{RT}$$

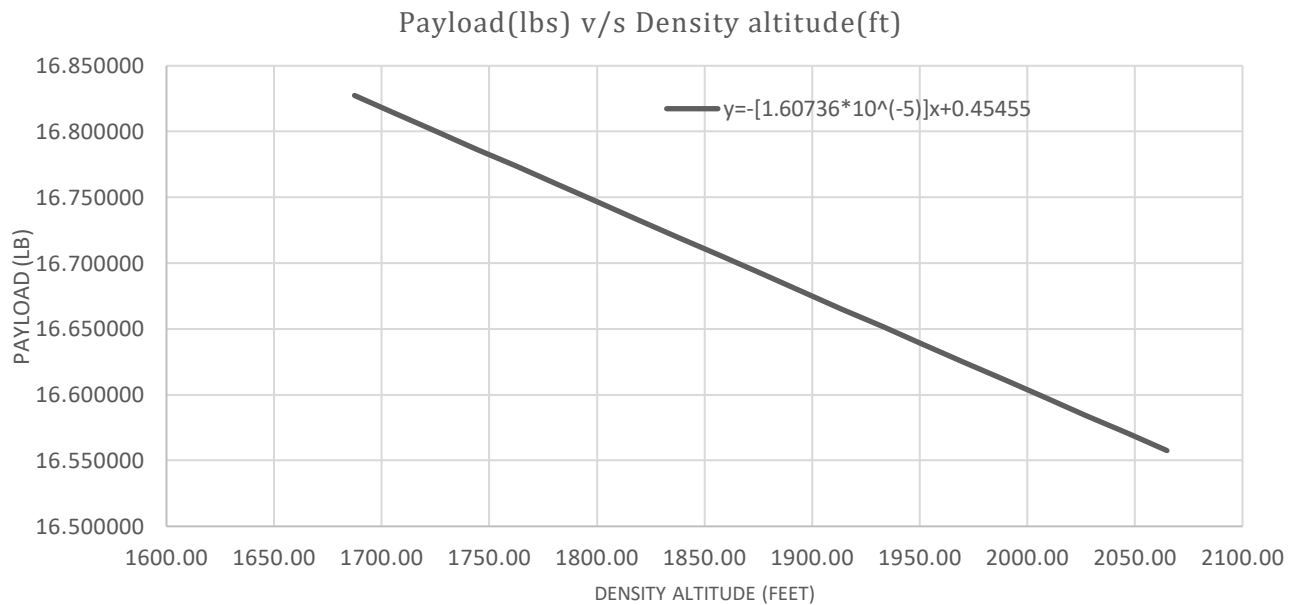


**Figure XXV** Payload prediction graph

The equation for Payload v/s Density altitude is  $y = 0.45455 - (1.60736 \times 10^{-5})x$

### 8.1. Conclusion

- 1) The graph between Density altitude (ft) and payload (lbs.) is linear with positive x and y-intercepts (Figure XXV ). Hence, the payload capacity decreases with an increase in density altitude.
- 2) The maximum payload carried at cruise can go up to 16.83 lbs.

### 9. Rib Spacing and Spar Location:

Specification	Values
Number of ribs – wing	40
Rib width	3 mm
Distance between two ribs	61.45 mm (equal spacing)
Aileron ribs	6
Number of ribs – fuselage	12 ( 4,4,4)
Middle section rib spacing	87.5, 78, 87.5 (mm)
Side section rib spacing	18, 18, 15 (mm)
Number of ribs – empennage	22
Distance between two ribs	37.53mm (equally spaced)
Elevator ribs	20
Rudder ribs	8
Distance between rudder ribs	37.87

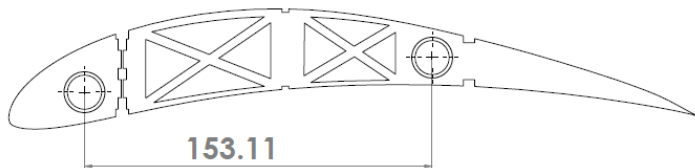


Figure XXVI Wing

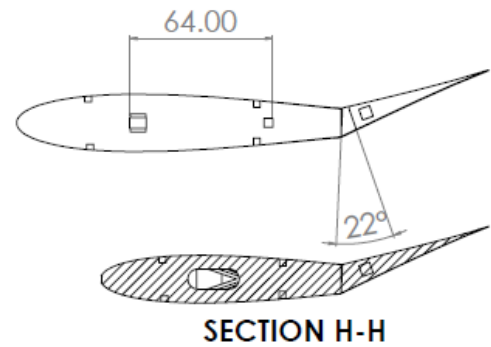


Figure XXVII Empennage

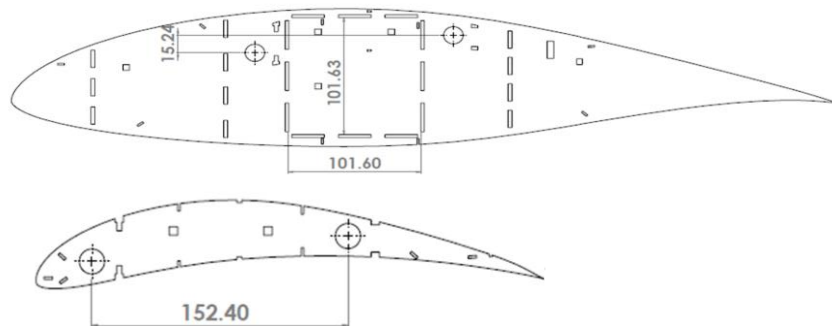


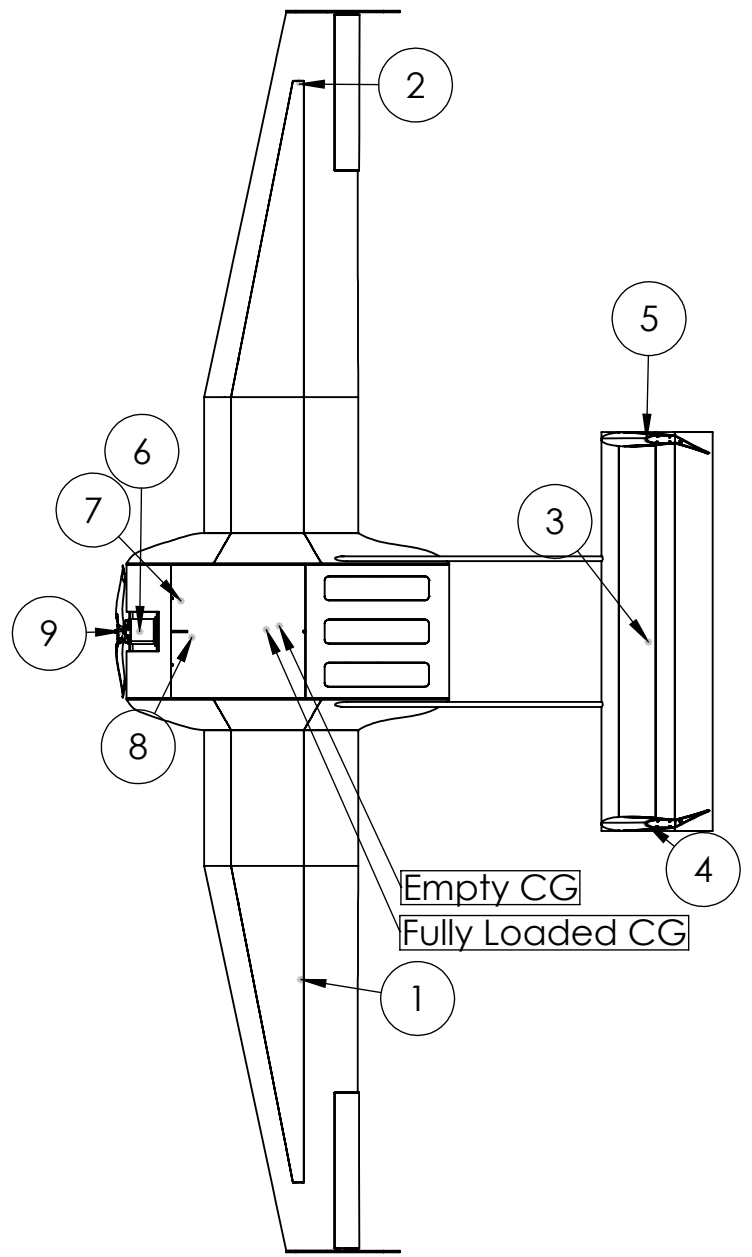
Figure XXVIII Fuselage

4

3

2

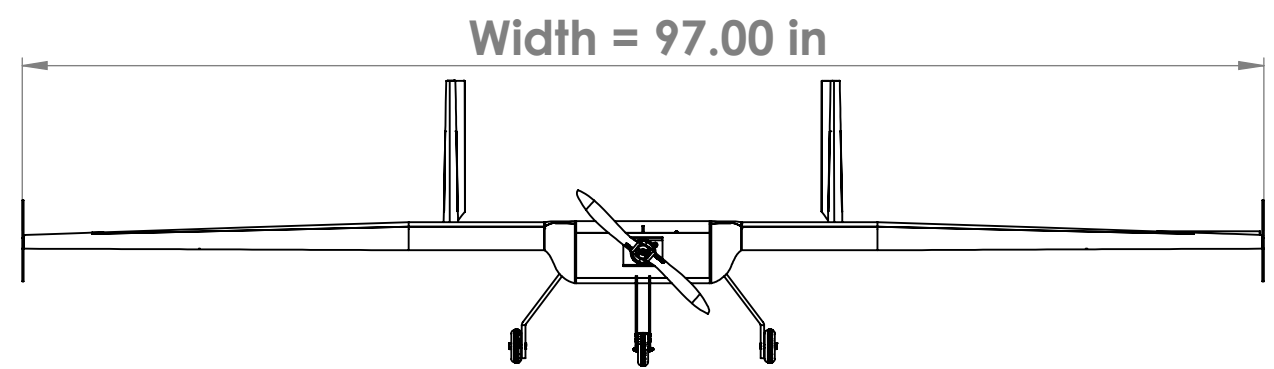
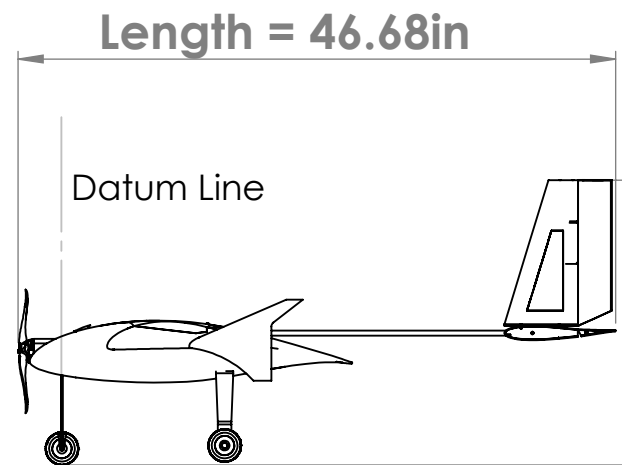
1



Component's CG Labels	Name	Mass (gram)	Distance from fully loaded CG (in)	Moment arm (in)	Moment (g-in <sup>2</sup> )
1	Left Wing Servo	11.20	42.48	11.03	1362.60
2	Right Wing Servo	11.20	42.48	11.03	1362.60
3	Elevator Servo	12.50	29.12	38.28	18316.98
4	Left Rudder Servo	13.40	33.14	38.14	19492.44
5	Right Rudder Servo	13.40	33.14	38.14	19492.44
6	Motor	398.00	10.71	-1.45	836.80
7	Battery	621.00	7.82	1.77	1945.53
8	ESC	63.00	6.70	2.62	432.46
9	Propellor	37.10	0.45	-2.93	318.50

S.no.	Property	Value
1	Wingspan	96.88 in
2	Empty Weight	3.425 kg
3	Motor KV	540
4	Propellor Diameter	14 in
5	Propellor Pitch	8.5 in

Empty CG  
Fully Loaded CG



<b>Team Name:</b> Phoenix Aero		
<b>Team no:</b>		
<b>Name of Institute:</b> Sardar Vallabhbhai National Institute of Technology, Surat		
SIZE <b>A3</b>	DWG. NO. <b>2D</b>	REV
SCALE: 1:15	WEIGHT: 3.425 kg	SHEET 1 OF 1

4

3

2

1

B

B

A

A

## 11. Conclusion

The SVNIT Phoenix Aero team completed a full conceptual study, a detailed technical review, and the development of a final design that fulfilled the Society of Automotive Engineers' specifications for the ISS Aero design competition. With no prior experience in designing a regular class aircraft, the team worked hard for eight months straight, never losing focus or motivation. The team is confident in their forecasting of flight efficiency and payload carrying ability. The “Xpartan” achieved its specified targets with a weight of just 3.425kg and a sleek, seamless body that could only be achieved with a dedicated team of Computer Aided Designers and technical members. The talents of each team member were emphasized, and work was assigned accordingly, resulting in a highly efficient aircraft design and analysis.

## References

- [1] Tulapurkara EG. Airplane design (Aerodynamic).
- [2] BÖTTGER O, TRAHMER B. Short Course Aircraft Design. Scholz D, editor. DGLR; 2007.
- [3] Sadraey MH. Tail design. Aircraft Design: A Systems Engineering Approach. 2013:274-352.
- [4] Lennon A. Basics of R/C model aircraft design: practical techniques for building better models. Motorbooks International; 1996.
- [5] Tulapurkara EG. Flight dynamics II-Airplane stability and control.
- [6] Maksoud TM, Seetloo S. Wingtips and multiple wing tips effects on wing performance: theoretical and experimental analyses. International Conference on Heat Transfer, Fluid Mechanics and Thermodynamics.
- [7] Deperrois A. XFLR5 Stability and Analysis.
- [8] Staples G. Propeller Static & Dynamic Thrust Calculation. Electric RC Aircraft Guy. 2013.
- [9] Atmosphere US. National oceanic and atmospheric administration. National Aeronautics and Space Administration, United States Air Force, Washington, DC. 1976 Oct.
- [10] Gadd C. Servo Torque Calculator. Calculate Required Servo Torque.